Effect of consolidation pressure on the impact behavior of UHMWPE composites

Authors: Torsten R. Lässig[a*], Michael May[a], Ulrich Heisserer[b], Werner Riedel[a], Frank Bagusat[a], Harm van der Werff[b], Stefan J. Hiermaier[a]

[a] Fraunhofer Institute for High Speed Dynamics, Ernst-Mach-Institut, Eckerstraße 4, D-79104, Freiburg, Germany.

[b] DSM Dyneema, P. O. Box 1163, 6160 BD Geleen, The Netherlands.

*Corresponding author

E-mail address: Torsten.laessig@emi.fraunhofer.de

Abstract

For the first time, the influence of the manufacturing process on the dynamic performance of ultra-high molecular weight polyethylene (UHMWPE, Dyneema® HB26) composites is investigated. The material is significantly influenced by the hot-pressing parameters temperature and pressure. The ballistic resistance and shock wave behavior was characterized for the UHMWPE composite consolidated with three different pressures. In the case of UHMWPE composites, higher consolidation pressures result in a better ballistic performance. The shock wave behavior converges to high-density polyethylene (HDPE). Based on these observations, an analytical approach is proposed describing the equation of state as a function of consolidation pressure.

Keywords: Polymer-matrix composites, Impact behavior, Consolidation

1. Introduction

Since the early 1960s, polymeric composites are a widely spread material class for ballistic protection systems due to their excellent strength to weight ratio and, therefore excellent impact resistance against a large field of threats. As an important representative, ultra-high molecular weight polyethylene (UHMWPE) composite, is used for personnel, vehicle and aircraft armor applications [1]. Its dynamic response, the deformation and fracture mechanisms caused by ballistic impact has extensively been characterized in recent years [2] [3] [4] [5] [6] [7] [8] [9] [10] [11] [12] [13] [14]. As all composite materials for protective applications, UHMWPE is subject to a continuous development for ballistic resistance and applicability in protective structures. It is generally known that the performance of composite structures is affected, amongst others, by morphological features such a pores, micro cracks in fibers or/and matrix or inclusions of foreign particles. These morphological features mostly trigger the initiation of failure and furthermore determine the quality of the composites mechanical properties. With regard to UHMWPE composites, the mechanical properties are not only dependent on the quality of its constituents such as the UHMWPE fibers or the matrix, but also on the manufacturing process [15]. The manufacturing process of UHMWPE composites [15, 16, 17], from gel-spun high-strength fibers up to consolidated biaxial oriented laminate plates, is displayed in Figure 1.

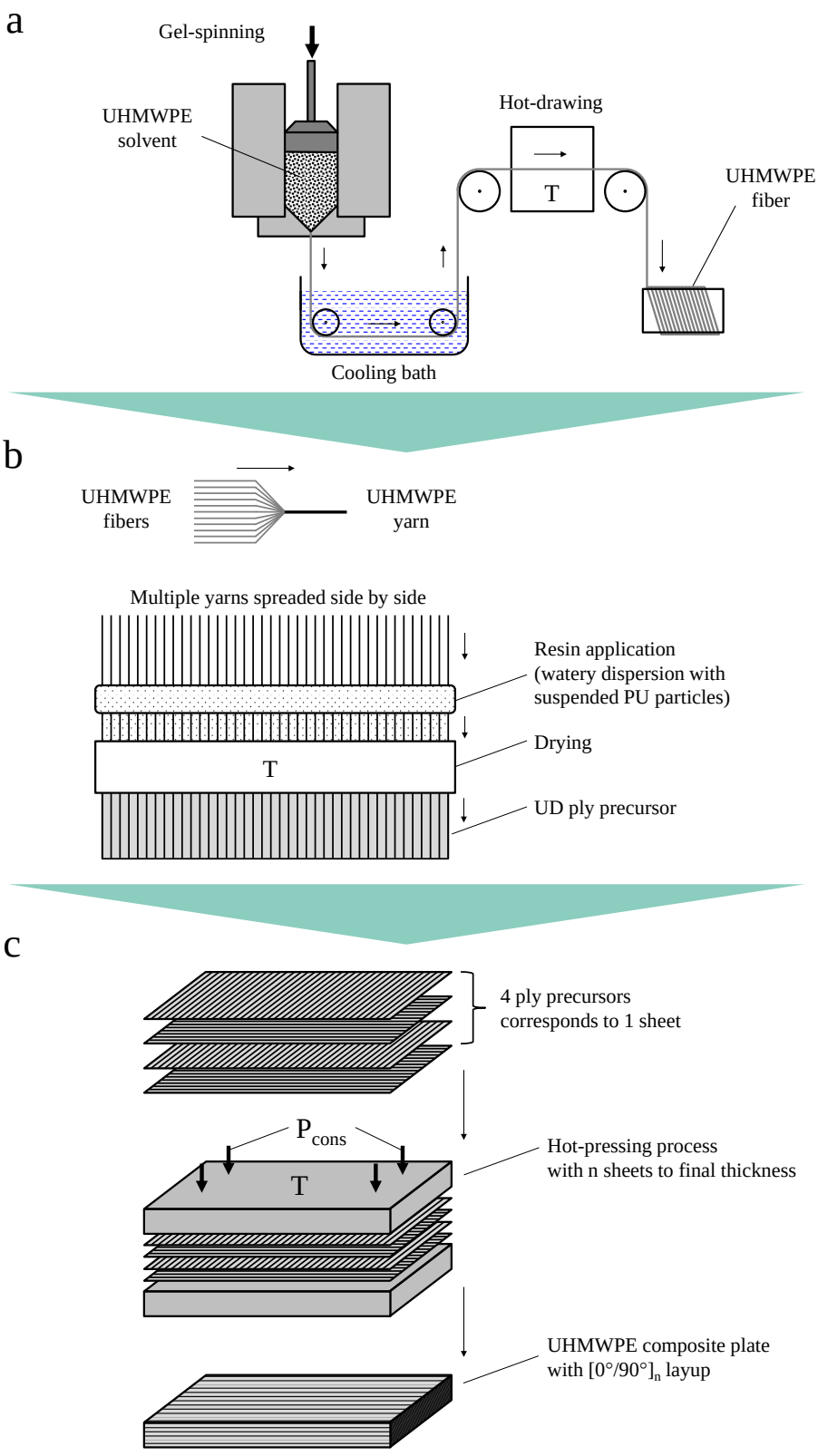

Figure 1: Manufacturing process of UHMWPE composites with a PU matrix, from gel-spun fibers (a) to unidirectional plies (b) cross plied to a sheet. These sheets are laid up and are finally hot-pressed to consolidated plates (c).

First, a UHMWPE fiber is extruded from a gel-like solvent, is cooled down to solid state and is subsequently hot-drawn (Figure 1, a). Multiple fibers are combined to yarns, which are placed next to one another in a layer. Then, the resin is applied using a watery dispersion with suspended polyurethane particles. The laminary compound is dried to a ply precursor (Figure 1, b). The last and plate forming manufacturing processes are a usually crosswise combination of ply precursors to sheets and the hot-pressing procedure of multiple sheets to the biaxial UHMWPE composite laminate (Figure 1, c). Thus, in conclusion with the remaining polyurethane (PU) particles a laminate with a non-continuous punctual PU-matrix is consolidated in the hot-pressing process.

In fact, the mechanical properties of the fibers in a composite are not noticeably affected by a variation of consolidation pressure, but inclusions of air (pores), pre-cracks of matrix, fraction of fiber-matrix or even fiber-fiber bonded joints are quantitatively influenced by the processing pressure. The effect of these morphological features on the mechanical properties of composite structures was intensively investigated in literature before [18, 19, 20, 21, 22, 23] and specifically for UHMWPE plates [15, 24] and are not discussed in form of a microscale analysis in this article. Additional information on the influence of the pressing process of UHMWPE composite plates and its parameters (pressure, temperature) is presented by Zheng et. al [25, 26].

The paper is organized as follows: Initially, classical ballistic experiments are described. In the following section, as an important mechanism during ballistic impact, the shock wave behavior is investigated by planar plate experiments. Finally, the influence of the consolidation pressure on the shock wave behavior of the UHMWPE composite is described by a new analytical approach.

2. Experimental investigation on the influence of consolidation pressures

In order to investigate the influence of the consolidation pressure on the material behavior of Dyneema® HB26 (consolidated at 20 bar, 165 bar, and 300 bar) under impact loading, two different types of experiments were carried out. On the one hand, ballistic impact tests with observations of depth of penetration and residual velocities (complete penetration) and on the other hand, inverse planar plate impact tests (PPI) for characterizing the shock response of UHMWPE were carried out.

2.1. Ballistic resistance

In this section, the influence of the consolidation pressure on the ballistic resistance is investigated. Ballistic experiments were carried out by impacting with C45-steel spheres of diameter 5.56 mm on UHMWPE target plates of size 100 x100 mm and an area density (AD) of 6 kg/m². The target was supported on a steel frame with circular aperture (diameter 70 mm). The tests were realized using a single-stage powder gun at DSM in the Netherlands. By increasing the impact velocity for each run, the increasing penetration depths and, for higher impact velocities, increasing residual velocities were recorded. The impact and residual velocities were measured using the calibrated Drello® light screens [27]. For the cases in which the projectiles were stopped, the specimens were cut open in the middle and the depth of penetration t_{DOP} was obtained by subtracting the thickness of the remaining undamaged layers in front of the projectile from the initial panel thickness like reported in [28]. A cross section of a UHMWPE plate after impact containing a stopped projectile and the used method of determination of the depth of penetration is shown in Figure 2.

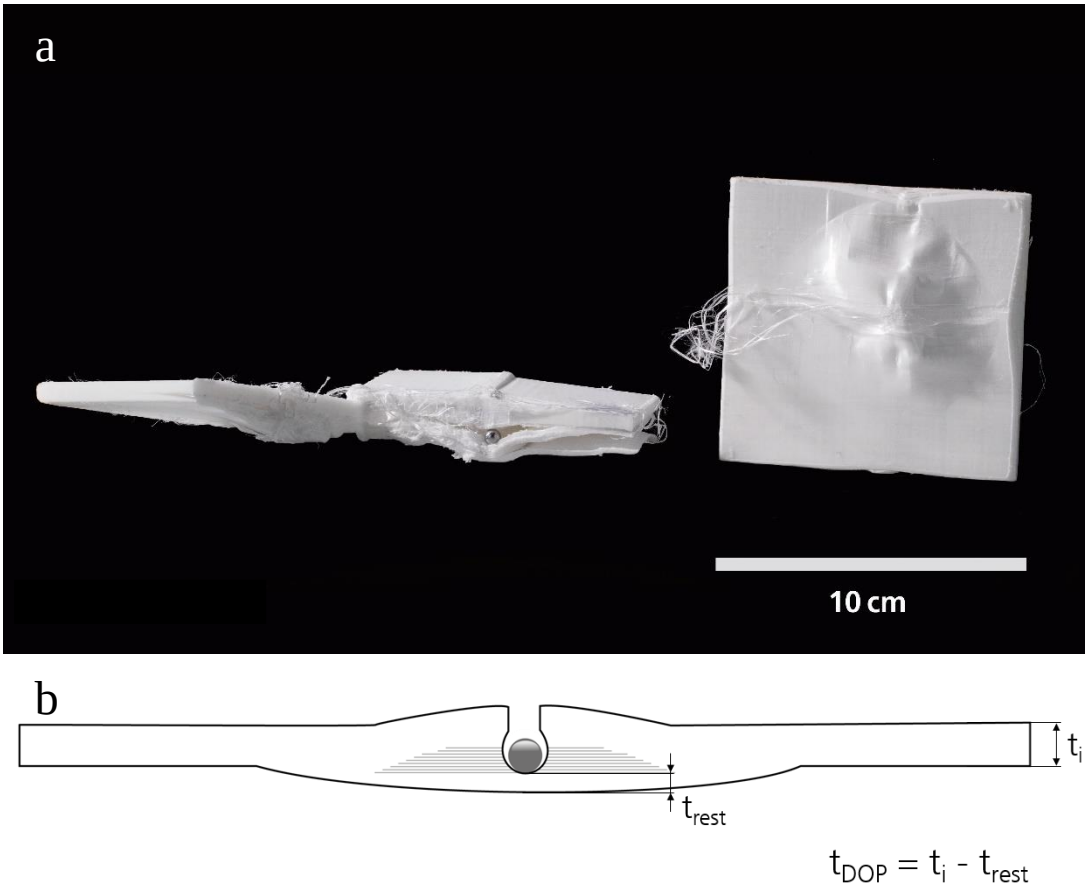

Figure 2: a) Section cut of a UHMWPE composite plate (area density = 6 kg/m²) with a stopped C45-steel sphere (Ø = 5.56 mm) and b) the depth of penetration determination method.

It was found in the cross sections that all characteristic deformation and damage mechanisms, that are well documented as energy absorbing mechanisms [2, 8, 9, 11, 24] occurred for each test with a stopped projectile. In the first section of the impact crater the layers were penetrated without delamination failure. In the remaining crater, the layers debonded by delamination failure in mode I and II [9]. The intact layers are not perforated but deformed both elastically and permanently. These mechanisms also cause the plates' typical back face bulge. The dominating mechanism for shaping of the back face bulge is delamination in mode I and mode II. This failure mechanism is controlled by the interlaminar strength. Due to the fact, that the level of interlaminar strength of laminated composites depends on the fiber-to-matrix interface, the difference between the results of the ballistic impact tests with specimens consolidated at 20 bar, 165 bar and 300 bar will be investigated. The before measured averaged thicknesses of the target specimen $t_{0,avg.}$ are reported in Figure 3 and Table 1.

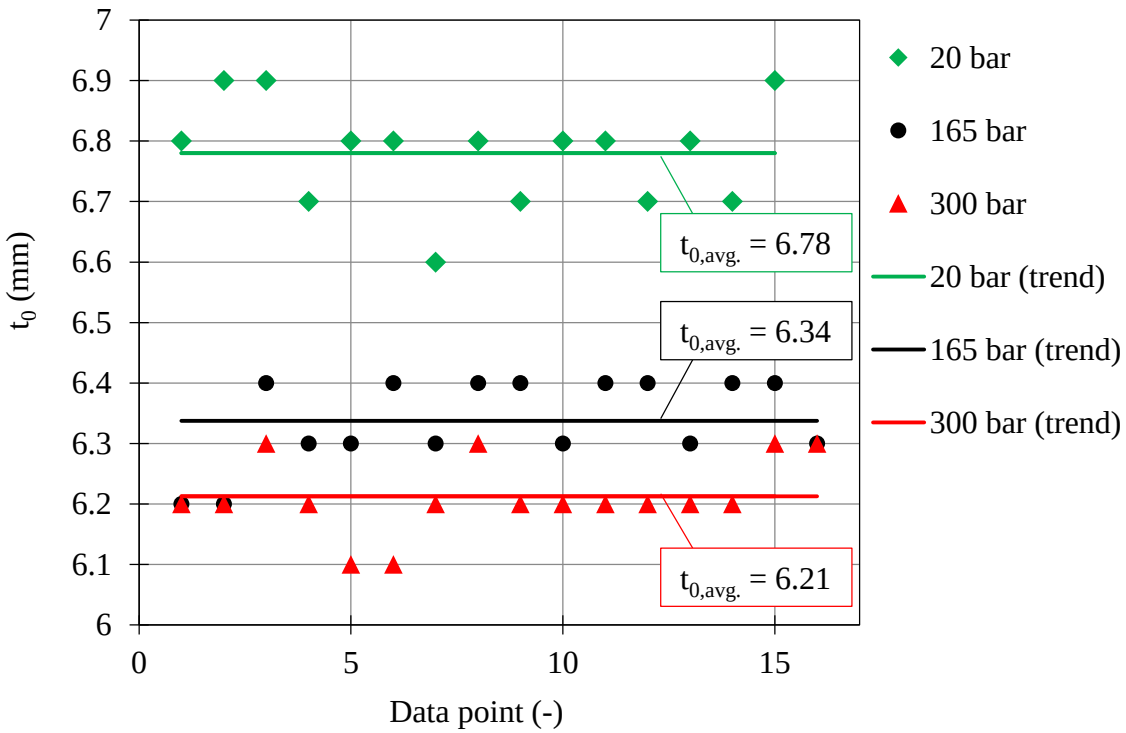

Figure 3: Influence of the consolidation pressure on the thickness t_0 of UHMWPE composite plates with an area density of 6 kg/m² pressed with 20 bar (green), 165 bar (black) and 300 bar (red).

The consolidation pressures of 20 bar, 165 bar or 300 bar resulted in averaged panel thicknesses of 6.78 mm, 6.34 mm or 6.21 mm, respectively (cf. Table 1). It was found that the average thickness and scatter decrease for higher consolidation pressures.

Table 1: Thicknesses of UHMWPE composite plates (area density = 6 kg/m²) hot-pressed with 20 bar, 165 bar and 300 bar.

Value: / Cons. pressure:	AD (kg/m²)	$\bar{x}_t$ (mm)	$\sigma_{\bar{x},t}$ (mm)	COV (%)	ρ (kg/m³)	$\Delta\rho_{rel.300}$ (%)
20 bar	6	6.78	0.0833	1.23	885	8.4
165 bar	6	6.34	0.0696	1.1	947	2.0
300 bar	6	6.21	0.0599	0.96	966	0

Here AD denotes the area density and $\bar{x}_t$ the average thickness for each consolidation pressure, accomplished by the standard deviation $\sigma_{\bar{x},t}$ the coefficient of variance COV the average density ρ and the density change $\Delta\rho_{rel300}$ relatively to plates consolidated with 300 bar.

The results of ballistic impact experiments for an impact velocity range of 600 m/s to 819 m/s are shown in Figure 4 and listed in Table 3.

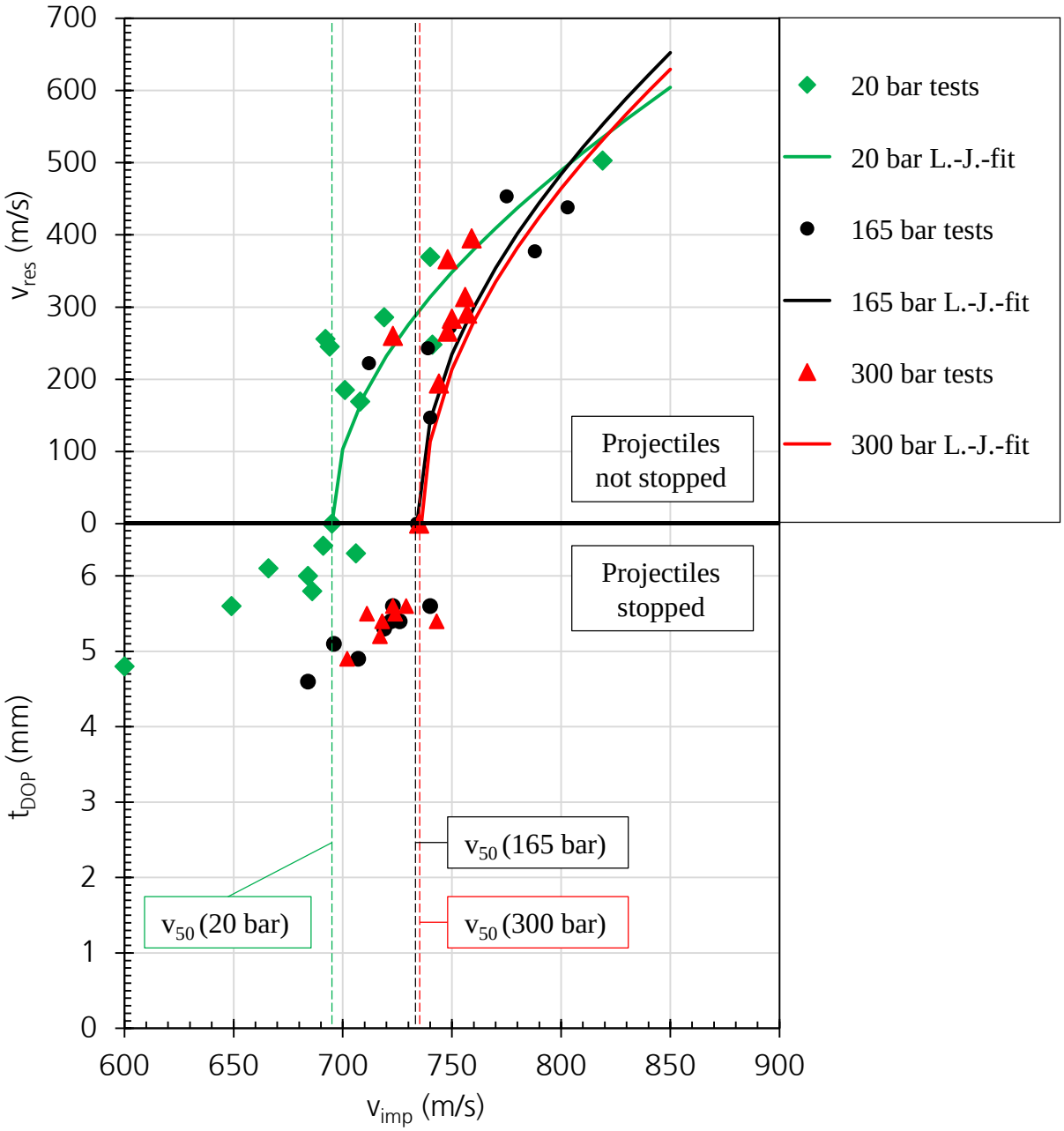

Figure 4: Depth of penetrations t_{DOP} for stops and residual against impact velocities v_{imp} of ballistic impact tests with steel spheres (Ø = 5.56 mm) on 100 x 100 mm² UHMWPE composite plates (AD = 6 kg/m²) hot-pressed with 20 bar (green), 165 bar (black) and 300 bar (red).

Figure 4 shows the results of the ballistic impact tests of UHMWPE composite target plates (AD = 6 kg/m²) impacted by hardened steel spheres (Ø = 5.56 mm). Plates pressed with 20 bar (green), 165 bar (black) and 300 bar (red) were used. In case of full penetrations, the

evolution of residual velocities was described by a Lambert-Jonas-formulation [29, 30], (Figure 4, above).

$$v_{res} = \alpha \cdot \left(v_{imp}^{p} - v_{bl}^{p}\right)^{\frac{1}{p}}, \text{ valid for } v_{imp} \geq v_{bl}. \quad (1)$$

Here, α is a constant parameter, p is an exponent and v_{bl} is the ballistic limit. For solid materials, p is usually set equal to 2 [30]. In this study, the standardized definition of the v_{50} is approximated by the value of v_{bl} that stands for the intersections of the axis abscissas (dashed lines) and the Lambert-Jonas-fits (solid lines). According to the standard [31], the v_{50} is the impact velocity of which a 50 % chance exist to stop the projectile. The fit of the formulation was carried out using an approximation implemented in the software GNUPLOT based on the Levenberg-Marquardt-algorithm [32, 33]. The determined parameter values for the Lambert-Jonas-fits for the results of 20 bar, 165 bar and 300 bar are summarized in Table 2:

Table 2: Parameter values for the Lambert-Jonas-formulation with p = 2 for obtained residual velocities of ballistic impact tests on UHMWPE composite plates (AD = 6 kg/m²), hot-pressed with consolidation pressures P_{con} of 20 bar, 165 bar and 300 bar, using hardened steel spheres (Ø = 5.56 mm).

Value	P_{con} = 20 bar	P_{con} = 165 bar	P_{con} = 300 bar
α	1.235	1.552	1.480
v_{bl}	695	734	736

The results of the residual velocities against impact velocities show an increase of the v_{50} between consolidation pressures of 20 bar and 300 bar. However, a comparison of the v_{50} value of 165 bar and 300 bar suggests that a further increase of the consolidation pressure will not significantly improve the v_{50} of UHMWPE composite plates against this type of projectile.

Table 3: Results of v_{50} determination of UHMWPE composite plates (AD = 6 kg/m²) pressed with 20 bar, 165 bar and 300 bar using hardened steel spheres (Ø = 5.56 mm).

Status of projectiles	v_{imp} (m/s)			Results (t_{DOP} / v_{res})			
	20 bar	165 bar	300 bar		20 bar	165 bar	300 bar
Projectiles stopped	706	740	743	t_{DOP} (m/s)	6.3	5.6	5.4
	691	726	729		6.4	5.4	5.6
	686	723	724		5.8	5.6	5.5
	684	722	723		6.0	5.4	5.6
	666	719	719		6.1	5.3	5.4
Projectiles not stopped	692	712	723	v_{res} (m/s)	256	222	260
	694	739	744		245	243	194
	701	740	748		185	147	266
	708	748	750		169	272	284
	719	775	749		286	453	366
v_{50} (m/s)	695	734	736				
$\lvert\Delta v_{50}\rvert$ (%)	5.31	-	0.27				

2.2. Shock response of UHMWPE composite plates under planar impact loading

The previous section showed an enhancement of ballistic resistance of UHMWPE composites with an increase of consolidation pressure. As an important indicator for ballistic impact predictions, mechanisms such as the behavior under shock loading must be investigated. In particular, the material state in front of and behind a shock wave must be considered. Typically, these states are described by the pressure, density and internal energy of the continuum material and are defined by the Rankine-Hugoniot conditions [34, 35] in terms of conservations of mass, momentum and energy, respectively. The one-dimensional shock response of a solid continuum material therefore satisfies Eqn. (2)-(4):

$$\rho_1 u_{P1} = \rho_0 u_{P0}, \tag{2}$$

$$P_1 + \rho_1 u_{p1} = P_0 + \rho_0 u_{P0}, \tag{3}$$

$$e_1 + \frac{P_1}{\rho_1} + \frac{u_1^2}{2} = e_0 + \frac{P_0}{\rho_0} + \frac{u_0^2}{2}. \tag{4}$$

Here, ρ is the density, u_p is the particle velocity, U_S is the shock velocity, e is the internal energy and P the pressure for a state change from state 0 to state 1 under one-dimensional shock loading. Following the Rankine-Hugoniot conditions, the adiabatic state change can be illustrated in the pressure-density-energy space (Figure 5).

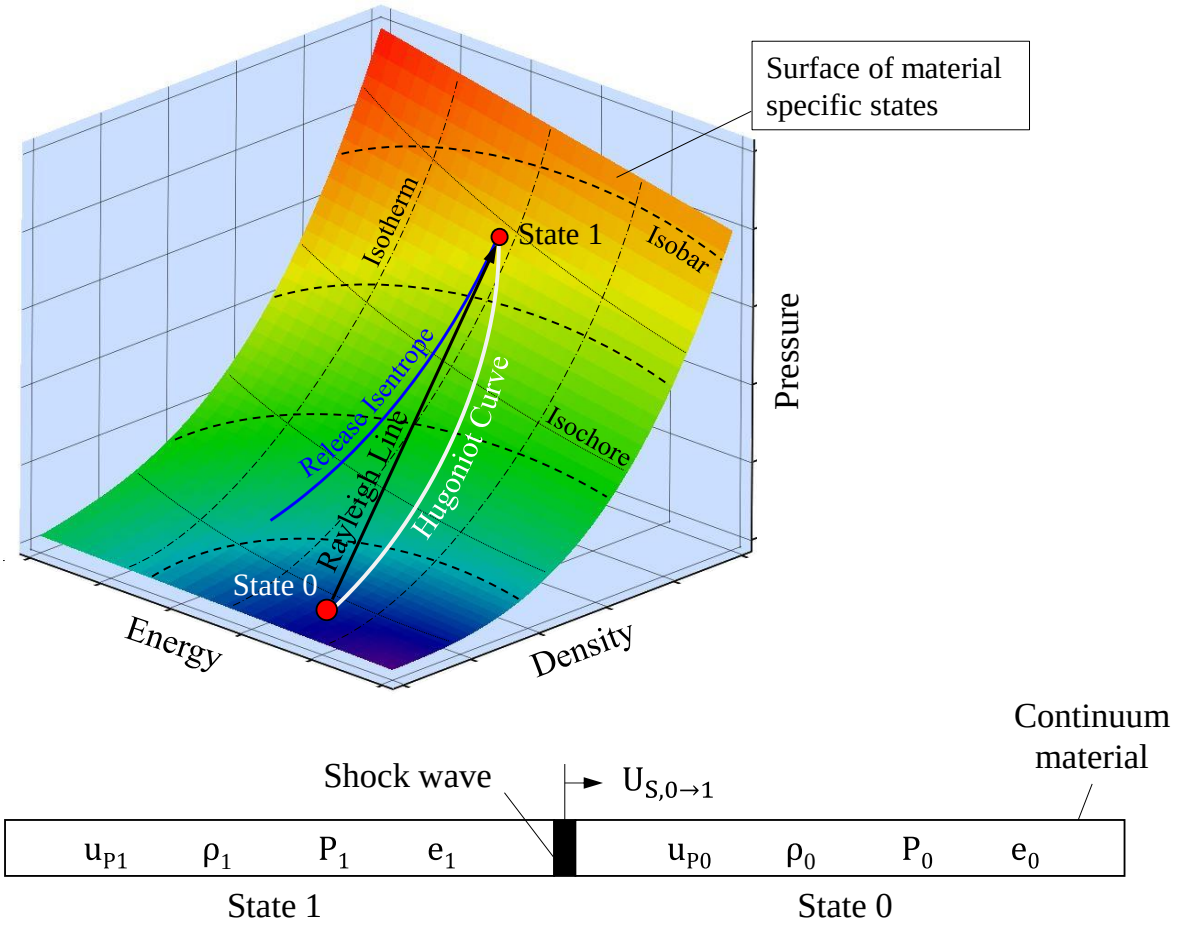

Figure 5: Equation of state surface in pressure-density-inner energy-space for material specific states; states that can be reached by shock loading (state 0 ➔ state 1) are marked by the Hugoniot Curve (white line).

The state change (0 → 1) in a continuum material under shock loading is illustrated by the Rayleigh Line (Figure 5) as an ideal jump condition. For a certain initial state 0 all accessible states caused by shock loading, depending on the intensity and initial state, are located on the material specific Hugoniot Curve. The three conservation equations (mass, energy and impulse, Eqn (2) – (4)) show four unknown parameters for state 1 (P_1, u_{P1}, ρ_1, e_1). Assuming the shock wave induced state change from 0 to 1 runs adiabatic (energy exchange is neglected), the system of conservation equations reduces to two equations containing three unknown parameters. However, the system of conservation equations (2), (3) is still under-determined. Hence, a further material specific constitutive relationship is required to determine a solution. Therefore, a shock equation of state (shock EOS) must be defined. Usually, a formulation for pressure as function of density and internal energy $P = f(\rho, e)$ is

used. In most cases, a shock velocity-particle velocity function $U_S = f(u_p)$ is used to approximate a shock EOS, due to the fact, that pressure, density and inner energy cannot be obtained directly after shock loading. A suitable experimental technique for observing the U_S-u_P-relationship is the planar plate impact (PPI) experiment.

In this study, the PPI tests in the inverse configuration are carried out using a single-stage accelerator (Figure 6).

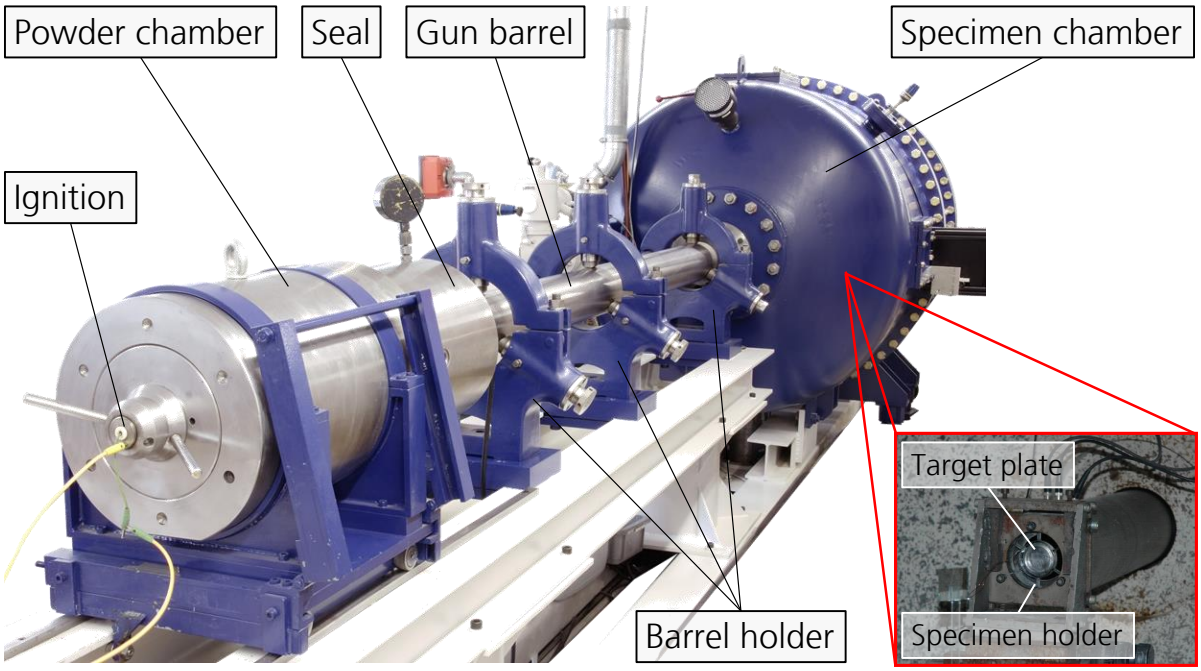

Figure 6: Single-stage (powder) accelerator for planar plate impact tests at EMI.

The inverse configuration of the planar plate impact test is commonly used if velocity measurements are technically difficult, due to poor reflectivity (pores, transparency, absorption effects) on the material surface to characterize ('observed surface', see *Figure 7*). This inverse configuration was also employed before, e. g. by [8, 10, 36, 37, 38] and was proved as a valid method for obtaining accurate shock data. Here, the plate of the material to characterize is sandwiched between two plates of material of known properties (C45 steel). Backing plates of thickness 5 mm, specimens of approximate thickness 6 mm (depending on consolidation pressure) and target plates of thickness 2.1 mm were used. The two bonded

projectile plates (backing and specimen) are carried by polycarbonate sabots and the target plates were fixed to stationary polycarbonate specimen holder. The impact velocity was measured by trigger pins in the gun barrel and the shock wave induced acceleration/velocity of the target's free surface was detected by a VISAR (velocity interferometer system for any reflector, [39, 40]). The scheme of the test setup is shown in Figure 7.

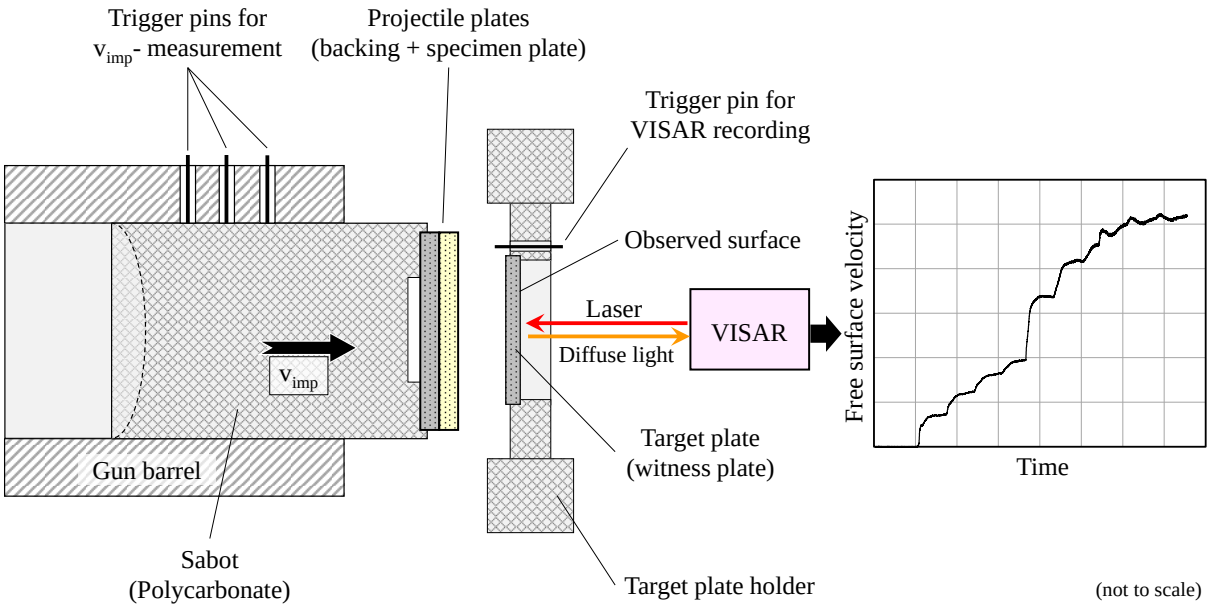

Figure 7: Test setup for planar plate impact tests in the inverse configuration using a single-stage accelerator and the VISAR system.

When the projectile plates hit the stationary target plate shock waves are induced causing specific shock states. Corresponding to the materials impedance Z, shock waves transmit (T) or reflect (R) from contact surfaces following Eqn. (5).

$$R = \frac{(Z_A - Z_B)}{Z_A + Z_B} \text{ and } T = \frac{2 \cdot Z_B}{Z_A + Z_B} \text{ for } R + T = 1 \text{ with } Z_i = \rho_i \cdot U_{S,i} \text{ with } i = A, B. \quad (5)$$

In Eq. (5) ρ is the density, $U_{S,i}$ is the shock velocity, indices A and B of the impedances Z_i refer to body A impacting body B, respectively. In general, A and B belong to different materials. A characteristic scheme (Lagrangian diagram) of the shock wave propagation for the selected plate configuration is illustrated in Figure 8 (left side) supplemented by the resulting velocity-history curve of the observed (free) surface (right side).

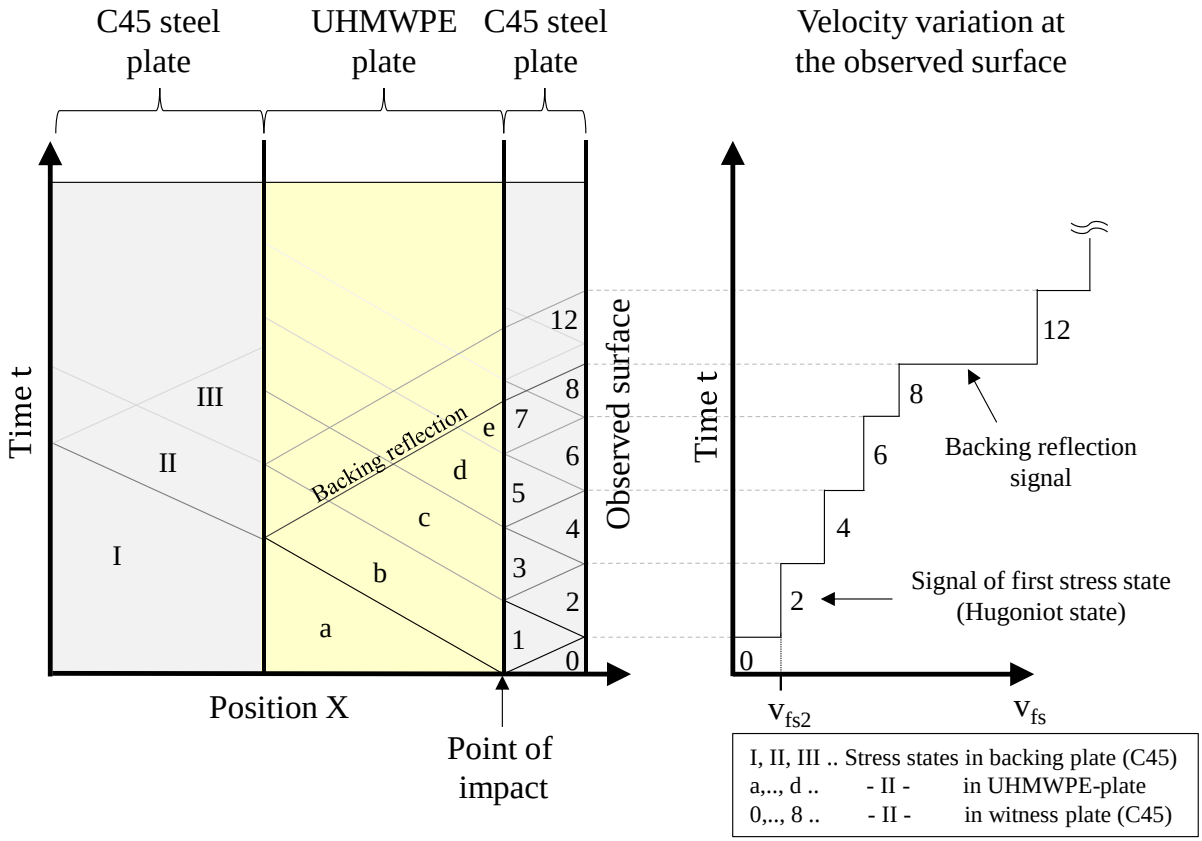

Figure 8: Characteristic scheme of shock wave propagation in an UHWMPE plate sandwiched between C45 steel plates after impact in inverse planar plate impact tests (left hand) and velocity variation at the observed surface (right hand).

From the point of impact shock waves propagate into the UHMWPE plate and the stationary C45 steel target plate (Figure 8, states 1 and b). Once the shock wave front in the target plate ends up at the free surface an acceleration of this surface can be recorded. The shock wave is then reflected at the free surface to a release wave causing state 2 in the target plate. Due to the higher impedance of steel compared to UHMWPE, the release wave is mostly reflected at the contact surface to a new compressive wave. Any arrival of a further compressive wave at

the free surface causes a new velocity plateau and, therefore, a new stress state (*Figure 8*, right side; see states 4, 6 and 8).

Due to the fact that the materials initial state is only known for the first stress state (Hugoniot state), the shock velocity-particle velocity relationship can only be calculated by evaluating the first velocity plateau of the free surface. This is due to the so called “free surface approximation”, which assumes that the velocity increase during release of the steel is approximately as high as the velocity increase during the shock transition before reflection [41]. However, this assumption is common for metals, therefore, steel as material for the witness plates and the planar plate impact test in the inverse configuration is used. Here, the particle velocity in the target plate caused by the shock wave is expressed as:

$$u_{P,C45} = \frac{u_{fs2}}{2}, \tag{6}$$

where u_{fs2} is the averaged value of the first free surface velocity plateau (Hugoniot state). The shock velocity in the target plate $U_{S,C45}$ is defined by Eq. (7).

$$U_{S,C45} = c_{B,C45} + S_{C45} \cdot u_{P,C45}. \tag{7}$$

Here, $c_{B,C45}$ is the bulk sound speed (4483 m/s, [42]) and S_{C45} is the linear slope coefficient (1.332, [42]) of C45 steel. Taking into account the velocity at the Hugoniot Elastic Limit of C45 steel ($u_{HEL,C45} = 75\ \mathrm{m/s}$, see measurements in [8, 43, 44]) the stress level of the first Hugoniot stress state in the target plate satisfies Eq. (8):

$$\sigma_h = \frac{1}{2}\rho_{0,C45} \cdot c_{B,C45} \cdot u_{HEL,C45} + \frac{1}{2}\rho_{0,C45} \cdot U_{S,C45} \cdot \left(u_{fs2} - u_{HEL,C45}\right). \tag{8}$$

On both sides of the impact surface continuity of stress ($\sigma_{h,C45} = \sigma_{H,UHMWPE}$) and particle velocity ($u_{P,C45} = u_{P,UHMWPE}$) is assumed. However, this is only valid before re-centering. After re-centering the particle velocity of the UHMWPE plate has to be calculated using Eq. (9) treating the UHMWPE plate as shocked from stationary conditions.

$$u_{P,UHMWPE} = v_{imp} - u_{P,C45} . \quad (9)$$

Following the conservation of momentum, Hugoniot stress in the UHMWPE plate is given by the linear relationship:

$$\sigma_h = \rho_{0,UHMWPE} \cdot U_{S,UHMWPE} \cdot u_{P,UHMWPE} . \quad (10)$$

Solving Eq. (10), the shock velocity of the UHMWPE plate $U_{S,UHMWPE}$ can be calculated. A detailed description to the calculation scheme can be found in [10, 36, 38, 45]. The results for analyzing the first Hugoniot stress state are summarized in Table 4.

Table 4: Hugoniot-data for UHMWPE composite plates, hot-pressed with 20 bar and 300 bar, obtained by inverse planar plate impact tests.

Test No.	P_{con} (bar)	v_{imp} (m/s)	u_{fs2} (m/s)	u_P (m/s)	σ_h (MPa)	$U_{S,Dyn}$ (m/s)
3702	20	380	29.9	365.3	668.2	1876.2
3703	20	248	14.6	240.6	336.4	1434
3705	20	547.4	58.3	518.5	1314.7	2600.6
3706	20	738	109.5	683.5	2359.8	3541.1
ma-748	20	1120	199.6	1020.2	3998.1	4428.1
3737	300	842	142.7	770.7	2963.7	3981.1
3738	300	664	98.8	614.6	2176.7	3666.2
3739	300	529	70	494	1590.1	3332.1
3741	300	234.1	26.5	220.8	603	2827
ma-749	300	1120	221.9	1009	4408	4522.2

Here, the 4-digit numbers show experimental results from inverse PPI tests using an impact facility with a 70 mm gun barrel. The results number starting with ‘ma-‘ were derived by an impact facility with a 52 mm gun barrel. The calculated results shown in *Table 4* base on the measured initial densities for UHMWPE plates consolidated with 20 bar and 300 bar listed in *Table 1*.

Additional Hugoniot data for UHMWPE composites pressed with 165 bar was taken from Lässig et al. [8, 10] and Chapman et al. [3]. Furthermore it is assumed that the U_S-u_P-data that is described by Chapman et al. [3] (grey dots) was obtained from UHMWPE composite plates pressed with the standard pressure of 165 bar although it is not specifically mentioned in the respective article. This is because his shock data lies directly within the scatter of the data from Lässig et al. [8, 10]. The results of the inverse PPI tests on UHMWPE composite plates, hot-pressed with 20 bar (green) and 300 bar (red), supplemented by results for 165 bar (black) and from literature ([3, 4], grey), are shown in Figure 9.

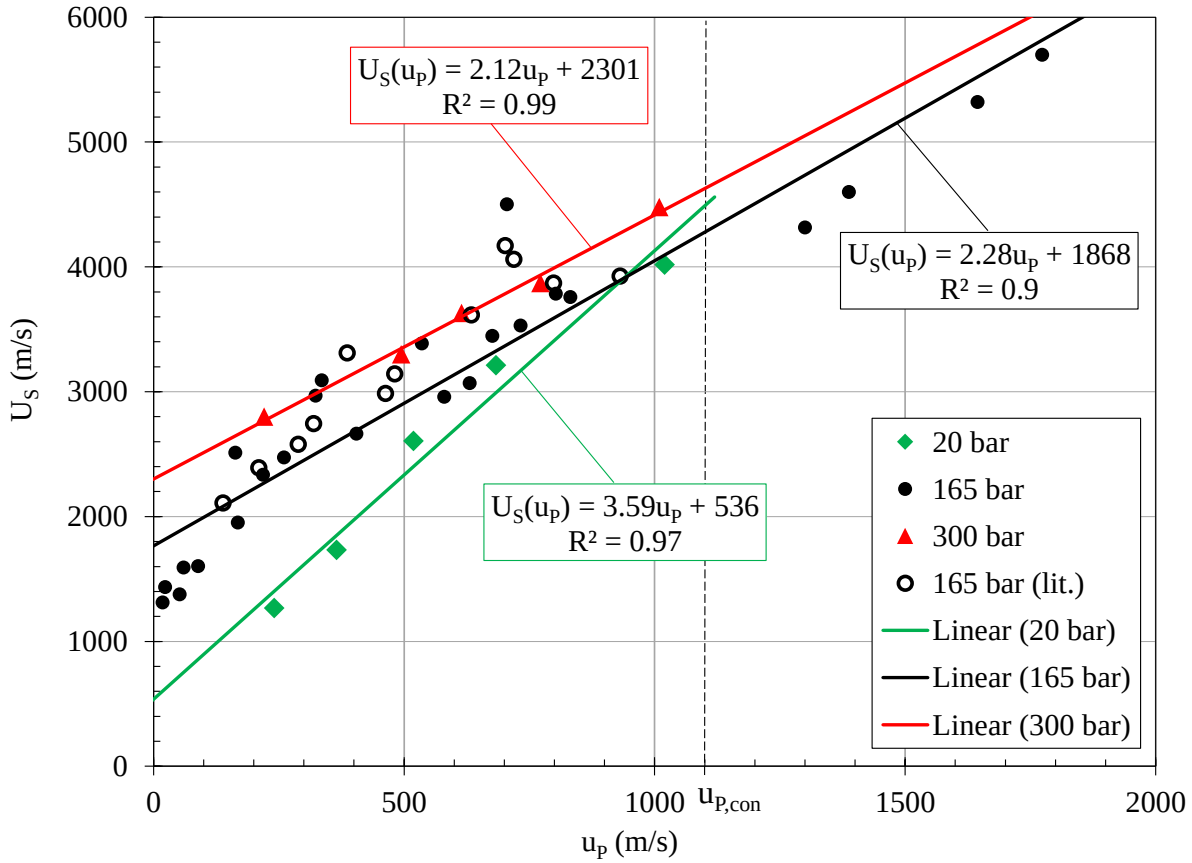

Figure 9: Results of inverse planar plate impact tests for consolidation pressures of 20 bar (green), 165 bar (black/grey) and 300 bar (red).

The PPI results for UHMWPE plates consolidated with 20 bar (green), 165 bar (black/grey) and 300 bar (red) were supplemented by linear trends of the form

$$U_S(u_P) = c_B + S \cdot u_P \quad \text{with} \quad \Gamma = 2 \cdot S - 1, \tag{11}$$

where Γ is the Mie-Grüneisen gamma. The results for c_B and Γ obtained from the linear trends (Figure 9) are listed in Table 5.

Table 5: Bulk sound speeds and Mie-Grüneisen gammas for UHMWPE composite plates hot-pressed with 20 bar, 165 bar and 300 bar, obtained by planar plate impact tests.

Consolidation pressure	c_B (m/s)	Γ (-)
20 bar	536	6.18
165 bar	1868	3.56
300 bar	2301	3.24

Figure 9 shows a clear influence of the consolidation pressure of Dyneema® HB26 composites below the particle velocity $u_{P,con}$ of 1100 m/s. Above this value, the shock-particle velocity relationship is assumed not to be sensitive to changes of consolidation pressures. Below $u_{P,con}$ the bulk sound speed increases and the Mie-Grüneisen gamma decreases for increasing consolidation pressures. For particle velocities between 200 m/s and 700 m/s, an influence of the consolidation pressure on the Hugoniot-data of UHMWPE composites can be observed. Concerning its constituents, UHMWPE composites consist of ultra-high molecular weight polyethylene fibers and a polyurethane matrix. Generally, the through-thickness properties of laminated thermoplastic composites are dominated, among others, by its matrix and morphological features of the microstructure. Therefore, the U_S-u_P-data investigated for UHMWPE composite plates pressed with three consolidation pressures is compared to data of representative isotropic polymers from Marsh ('LASL', [46], Figure 10). Figure 10 should clarify, if the through-thickness shock response of UHMWPE composites approach these of polyethylene (fibers) or polyurethane (matrix).

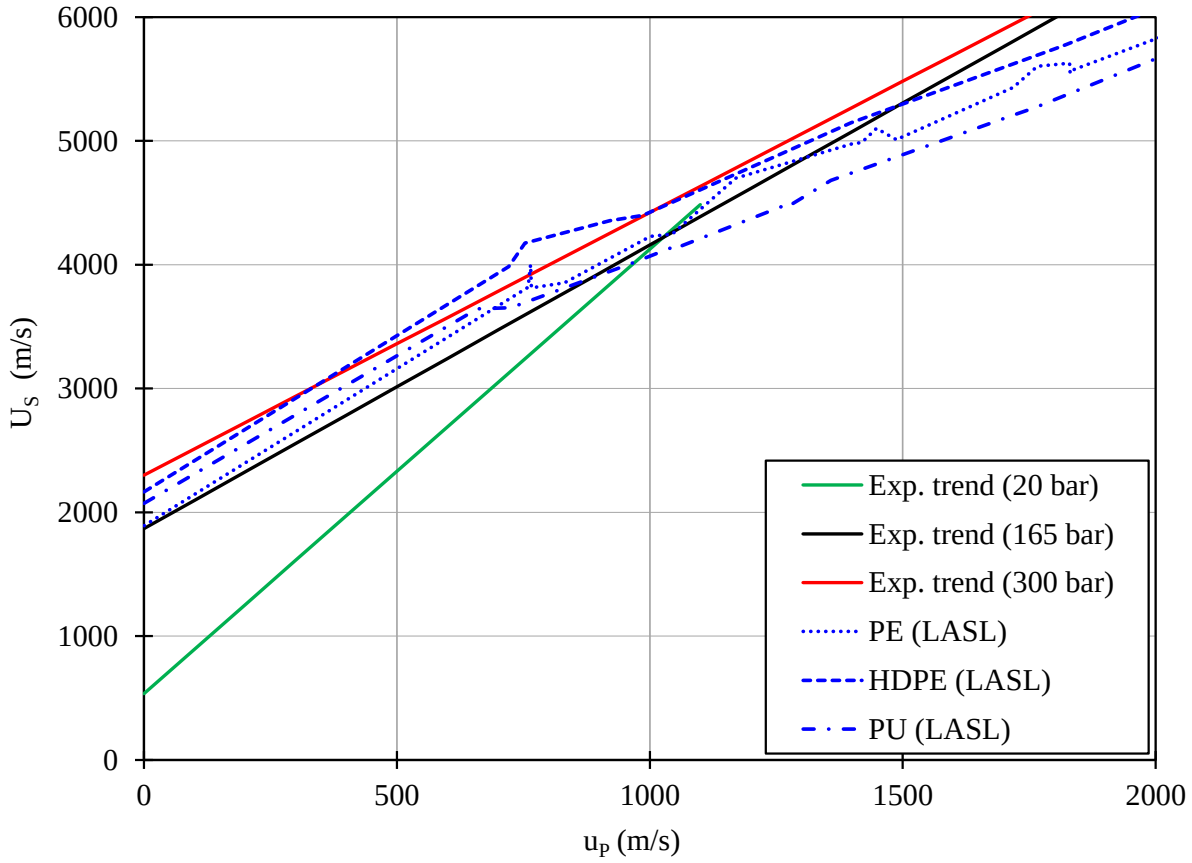

Figure 10: Overview of averaged U_S-u_P-curves of UHMWPE composites for three different consolidation pressures compared to results of pure polyethylene (PE), high-density polyethylene (HDPE) and polyurethane (PU) from literature [46].

In Figure 10 the results of this study are compared to shock velocity-particle velocity relations of isotropic polyethylene (PE), high-density polyethylene (HDPE) and polyurethane (PU), marked as blue dashed and dotted lines. In contrast to the assumption that the through-thickness shock wave behavior is adapting upon consolidation to the U_S-u_P-data of the PU matrix of UHMWPE plates, cannot be confirmed in terms of increasing the consolidation pressure. Moreover, by increasing the consolidation pressure, the U_S-u_P-relation of UHMWPE composites further resembles to the shock data of HDPE. It can be assumed that the influence of the PU matrix is decreasing higher pressures. However, it is strongly assumed, that further increase of the consolidation pressure (above 300 bar) will converge the shock response of the UHMWPE composite material towards or even exceed homogeneous high-density polyethylene.

3. Analytical approach

In section 2.3 inverse PPI tests were carried out to investigate the influence of consolidation pressures of 20 bar, 165 bar and 300 bar on the shock wave behavior. According to the results of the ballistic impact tests in section 2.2 could be pointed out, that higher consolidation pressures improve the capability for energy absorption especially for impact velocities below 1100 m/s, due to the higher level of the U_S-u_P-relation. It is assumed that the influence of the consolidation pressure on the shock behavior for impact velocities above 1100 m/s is closely negligible. Therefore, the linear trend of the UHMWPE composite plates pressed with 300 bar, which is nearly congruent to the U_S-u_P-relation of HDPE, will be used as piecewise formulation. The bulk sound speed c_B for particle velocities below 1100 m/s $u_{P,IPP}$ therefore can be expressed as a logarithmic function of consolidation pressure P_{con} Eq. (12). The logarithmic term should express the decreasing effect of higher consolidation pressures. The linear part (constant b) is needed in order to reach the value of c_B for the lowest consolidation pressure (20 bar).

$$c_B = f(P_{con}) = a \cdot \ln(P_{con}) + b, \tag{12}$$

where a and b are independent constants. Due to the bilinear slope of the U_S-u_P-relationship of the slope coefficient S below the particle velocity $u_{P,con}$ a piecewise defined function is used:

$$S = f(P_{con}) = \begin{cases} c \cdot \ln(P_{con}) + d & \text{for } u_P \leq u_{P,con}, \\ S_{300} \approx S_{HDPE} & \text{otherwise}. \end{cases} \tag{13}$$

where c and d are independent constants. The first equation describes the consolidation pressure dependent slope of the U_S-u_P-relationship and the second equation specifies the linear slope that equals the slope of UHMWPE pressed with 300 bar or of HDPE,

alternatively. With the linear equation for the bulk sound speed and the piecewise definition for the slope coefficient S the definition for the shock velocity U_S can be satisfied by Eq. (14):

$$U_S = f(u_P, P_P) = \begin{cases} [a \cdot \ln(P_{con}) + b] + u_P [c \cdot \ln(P_{con}) + d] & \text{for} \quad u_P \le u_{P,con}, \\ c_{B,300} + u_P \cdot S_{300} & \text{otherwise} \ . \end{cases} \tag{14}$$

The independent constants a – d are determined by calibrating the bulk sound speed c_B and the slope coefficient S against the experiments. This analytically formulated, consolidation pressure dependent U_S-u_P-relationship for UHMWPE composites for a range of 20 bar up to 300 bar is drawn against the linear, experimental trends and is displayed in Figure 11.

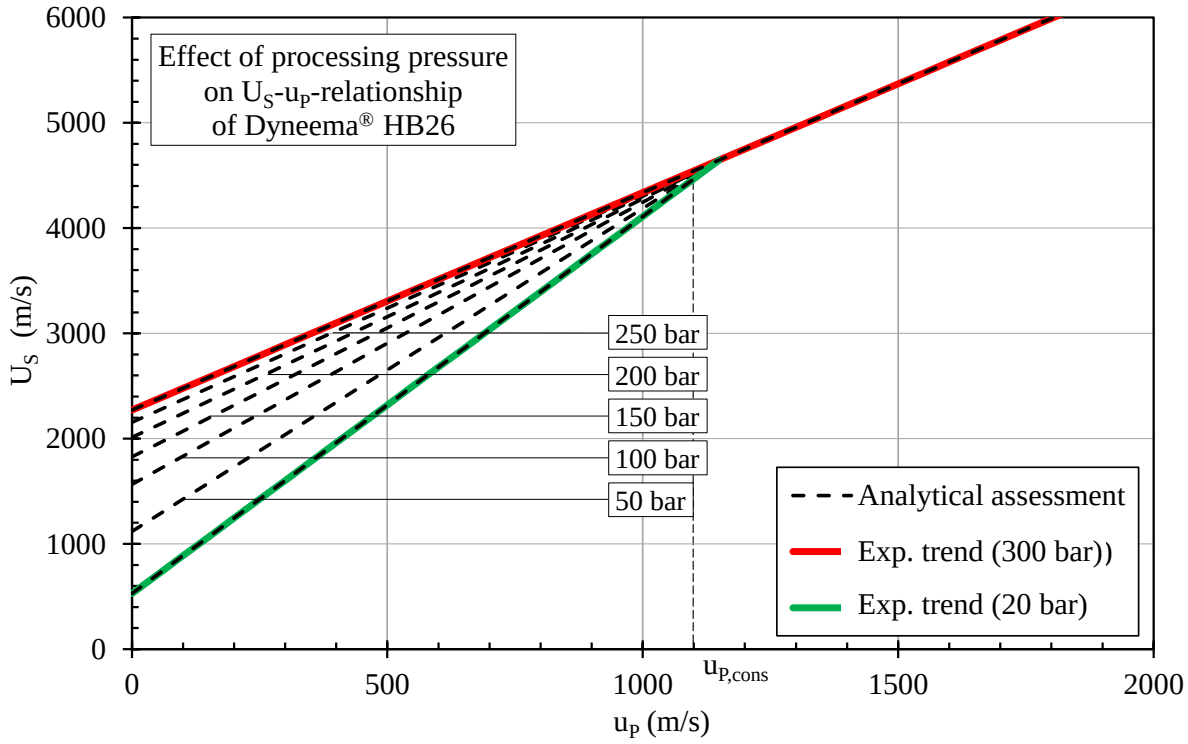

Figure 11: Analytical assessment for the U_S-u_P-relationship of UHMWPE composite plates for consolidation pressures of 20 up to 300 bar compared to the experimental trends (solid lines).

The experimentally obtained trends of the U_S-u_P-relationship for two consolidation pressures (20 bar (green), 300 bar (red)) defines the range of the semi-analytical approach that is supplemented incrementally for pressure steps of 50 bar (dashed lines). The obtained constants a – d (Eq. (14)) for the investigated UHMWPE composite material are listed in Table 6.

Table 6: Values for the constants in the consolidation pressure dependent formulation of the U_S-u_P-relationship of a UHMWPE composite for the pressure range of 20 bar up to 300 bar.

Constant	a	b	c	d
Value (-)	644	1401	-0.56	5.26

The formulation presented in Eq. (14) is valid for a range of consolidation pressures of 20 bar to 300 bar.

4. Conclusions

In this study, the effect of the manufacturing pressure on the ballistic impact resistance and the shock wave behavior of UHMWPE (Dyneema® HB26) composites is investigated. The effect of the consolidation pressure on the behavior under impact loading is verified by ballistic tests, evaluating depth of penetration and v_{50} and, in terms of shock wave transmissions, the planar plate impact test (in the inverse configuration) for an UHMWPE composite material. It was found that the depth of penetration of UHMWPE composites is reduced and the v_{50} velocity value is increased by higher consolidation pressures. This effect levels off at higher pressures. For ballistic impact situations with very high impact velocities, material specific shock wave phenomena become a more and more important mechanism during energy dissipation. To that aim, planar plate impact tests up to impact velocities above 1000 m/s were carried out. It was found that the U_S-u_P relationship do not appear as a continuous linear trend for different consolidation pressures. Especially, for particle velocities below 1100 m/s the U_S-u_P-curves were at a lower level but steeper slope for lower consolidation pressures. The bulk sound speed is increased and the Mie-Grüneisen gamma decreased as a result of higher consolidation pressures during the hot-pressing process of UHMWPE composites. This material specific behavior is measured, described and interpreted for this material class for the first time.

For practical application, an analytical and numerical approach is presented that quantifies this effect and enables realistic predictions of the shock wave behavior of UHMWPE composite materials.

Another aspect not investigated here but deserving attention is the observation that with higher consolidation pressure the mode II interlaminar shear strength is found to be reduced [47]. A new methodology to derive the interlaminar shear strength of UHMWPE plates is introduced in [48].

This study demonstrates that the influence of manufacturing parameters on the behavior under high velocity impact and, therefore, the ballistic performance and resistance of this class of composite materials deserves further investigations, e.g. concerning its spallation failure behavior.

Acknowledgements

The authors would like to thank Mr. Siegfried Pfändler and Mr. Michael Maurer from EMI for the extensive material planar plate testing and Dr. Hartwig Nahme for his supportive expertise in shock physics, and hence, many enriching discussions. The help of the DSM Dyneema Technicum for pressing the plates and ballistic testing is gratefully acknowledged.

Dyneema®, the world's strongest fiber™, is a DSM trademark for Ultra High Molecular Weigt Polyethylene (UHMWPE) fibers.

References

[1] H. van der Werff and U. Heisserer, "High-performance ballistic fibers: ultra-high molecular weight polyethylene (UHMWPE)," in *Advanced Fibrous Composite Materials for Ballistic Protection*, Woodhead Publishing, 2016, pp. 71-107.

[2] M. J. Iremonger, "Polyethylene Composites for Protection against High Velocity Small Arms Bullets," in *Proceedings of the 18th International Symposium on Ballistics*, San Antonio, TX, 1999.

[3] D. J. Chapman, C. H. Braithwaite and W. G. Proud, "The response of Dyneema® to shock-loading," American Institute of Physics, Cambridge, UK, 2009.

[4] H. Nahme, "Dynamic Properties of Dyneema® Plastic Material, EMI-Report No. E12/00," Freiburg, Germany, 2000.

[5] P. J. Hazell, G. J. Appleby-Thomas, X. Trinquant and D. J. Chapman, "In-fiber shock propagation in Dyneema®," *J. Appl. Phys.*, no. 110, p. 043604, 2011.

[6] T. Lässig, W. Riedel, U. Heisserer, H. van der Werff, M. May and S. J. Hiermaier, "Numerical sensitivity studies of a UHMWPE composite for ballistic protection," in *WIT Transactions on the built environment*, Ashurst, Southampton, UK, 2014.

[7] A. S. Fallah, K. Micallef, G. S. Langdon, W. C. Lee, P. T. Curtis and L. A. Louca, "Dynamic response of Dyneema® HB26 plates to localised blast loading," *Int. J. Impact Eng.*, vol. 73, pp. 91-100, 2014.

[8] T. Lässig, L. Nguyen, M. May, W. Riedel, S. Hiermaier, U. Heisserer and H. van der Werff, "A non-linear orthotropic hydrocode model for ultra-high molecular weight polyethylene in impact simulations," *Int. J. Impact. Eng.*, vol. 75, pp. 110-122, 2015.

[9] L. H. Nguyen, S. Ryan, S. J. Cimpoeru, A. P. Mouritz and A. C. Orifici, "The effect of target thickness on the ballistic performance of ultra high molecular weight polyethylene composite," *Int. J. Impact. Eng.*, vol. 75, pp. 174-183, 2015.

[10] T. Lässig, F. Bagusat, M. May and S. Hiermaier, "Analysis of the shock response of UHMWPE composites using the inverse planar plate impact test and the shock reverberation technique," *Int. J. Impact Eng.*, no. 86, pp. 240-248, 2015.

[11] L. H. Nguyen, T. R. Lässig, S. Ryan, W. Riedel, A. P. Mouritz and A. C. Orifici, "A methodology for hydrocode analysis of ultra-high molecular weight polyethylene composite under ballistic impact," *Compos. Part A-Appl. S.*, vol. 84, pp. 224-235, 2016.

[12] H. van der Werff, U. Heisserer, T. Lässig and W. Riedel, "From a hydrocode model of Dyneema® HB26 to radically improved armor," in *Proceedings of the 28th International Symposium on Ballistics*, Atlanta, USA, 2014.

[13] M. May and T. Lässig, "Rate-dependent mode I delamination in ballistic composites – Experiment and simulation," *Compos. Struct.*, vol. 180, pp. 596-605, 2017.

[14] T. Lässig, F. Bagusat, S. Pfändler, M. Gulde, D. Heunoske, J. Osterholz, W. Stein, H. Nahme and M. May, "Investigations on the spall and delamination behavior of UHMWPE composites," *Compos. Struct.*, vol. 182, pp. 590-597, 2017.

[15] B. P. Russell, K. Karthikeyan, V. S. Deshpande and N. A. Fleck, "The high strain rate response of ultra high molecular-weight polyethylene: From fiber to laminate," *Int. J. Impact Eng.*, vol. 60, pp. 1-9, 2013.

[16] P. Smith, P. J. Lemstra, B. Kalb and A. J. Pennings, "Ultrahigh-strength polyethylene filaments by solution spinning and hot drawing," *Polym. Bull.*, vol. 1, pp. 733-736, 1979.

[17] P. Smith and P. J. Lemstra, "Ultra-high-strength polyethylene filaments by solution spinning/drawing," *J. Mater. Sci.*, vol. 15, pp. 505-514, 1980.

[18] K. Senthil, A. Arockiarajan, R. Palaminathan, B. Santhosh and K. M. Usha, "Defects in composite structures: Its effects and prediction methods - A comprehensive review," *Compos. Struct.*, vol. 106, 2013.

[19] S. L. Lemanski, J. Wang, M. Sutcliffe, K. D. Potter and M. R. Wisnom, "Modelling failure of composite specimens with defects under compression loading," *Compos. Part A-Appl. S.*, vol. 48, pp. 26-36, 2013.

[20] Y. Gowayed, G. Ojard, E. Prevost, U. Santhosh and G. Jefferson, "Defects in ceramic matrix composites and their impact on elastic properties," *Compos. Part B-Eng.*, vol. 55, pp. 167-175, 2013.

[21] A. P. Mouritz and R. S. Thomson, "Compression, flexure and shear properties of a sandwich composite containing defects," *Compos. Struct.*, vol. 44, pp. 263-278, 1999.

[22] K. Croft, L. Lessard, D. Pasini, M. Hojjati, J. Chen and A. Yousefpour, "Experimental study of the effect of automated fiber placement induced defects on performance of composite laminates," *Compos. Part A-Appl. S.*, vol. 42, pp. 484-491, 2011.

[23] R. A. Garrett, "Effects of defects on aircraft composite structures," Defense Technical Information Center, St. Louis, USA, 1983.

[24] M. R. O'Masta, D. H. Crayton, V. S. Despande and H. N. G. Wadley, "Mechanisms of penetration in polyethylene reinforced cross-ply laminates," *Int. J. Impact. Eng.*, vol. 86, pp. 249-264, 2015.

[25] Z. Zheng, X. Huang, Y. Li, N. Yang, X. Wang and M. Shi, "Influence factors of internal structure and interfacial compatibility of UHMWPE fiber/SEBS resin composites: Processing parameters, structure of fiber and nature of resin," *Composites Part B,* vol. 43, pp. 1538-1544, 2012.

[26] Z. Zheng, G. Bingbing, M. Li, J. Li and X. D. Zhou, "Experimental and simulated investigation of temperature distribution of UHMWPE laminated composites during hot pressing process," *J. Appl. Polym. Sci.*, vol. 135, p. 45874, 2018.

[27] D. LS23-F1, "http://www.drello.de/downloads/ballistic/pdf/LS23_EN.pdf," [Online].

[28] U. Heisserer, H. Van der Werff and J. Hendrix, "Ballistic depth of penetration studies in Dyneema® composites," in *Proceedings of the 27th International Symposium on Ballistics*, 2013.

[29] J. P. Lambert and G. H. Jonas, "Report BRL-R-1852," Aberdeen, Maryland, USA, 1976.

[30] R. F. Recht and T. W. Ipson, "Ballistic perforation dynamics," *ASME J. Appl. Mech.*, pp. 384-390, 1963.

[31] MIL-STD-662F, "V50 Ballistic test test for armor," U.S. Army Research Lab, Aberdeen Proving Ground, USA, 1997.

[32] K. Levenberg, "A Method for the Solution of Certain Problems in Least Squares," *Quart. Appl. Math. 2*, pp. 164-168, 1944.

[33] D. Marquardt, "An Algorithm for Least-Squares Estimation of Nonlinear Parameters," *SIAM. J. Appl. Math. 11*, pp. 431-441, 1963.

[34] W. J. M. Rankine, "On the thermodynamic theory of waves of finite longitudinal disturbances," *Phil. Trans. R. Soc. B,* vol. 160, pp. 277-288, 1870.

[35] H. Hugoniot, "Mémoire sur la propagation des mouvments dans les corps et spécialement dans les gaz parfaits (première partie) [Memoir on the propagation of movements in bodies, especially perfect gases (first part)]," *J. Ec. Poly.*, vol. 57, pp. 3-97, 1889.

[36] M. A. Meyers, Dynamic behavior of materials, New York: John Wiley & Sons, 1994.

[37] D. E. Grady, "Impact Compression Properties of Concrete," 6th Symposium on Interaction of Nonnuclear Munitions with Structures, Panama City, Florida, USA, 1993.

[38] T. Hoerth, F. Bagusat and S. Hiermaier, "Hugoniot data of Seeberger sandstone up to 7 GPa," *Int. J. Impact Eng.*, vol. 99, pp. 122-130, 2017.

[39] L. M. Barker and R. E. Hollenbach, "Laser interferometer for measuring high velocities of any reflecting surface," *J. Appl. Phys.*, vol. 43, pp. 4669-4675, 1972.

[40] L. M. Barker and K. W. Schuler, "Correction to the velocity-per-fringe relationship for the VISAR interferometer," *J. Appl. Phys.*, pp. 3692-3693, 1974.

[41] J. R. Asay and M. Shahinpoor, High-Pressure Shock Compression of Solids, Springer New York, 1993.

[42] H. Nahme, "Equation of state measurement of 9SMn28-C45-Steel," Freiburg, 1991.

[43] I. Rohr, H. Nahme and K. Thoma, "Material characterization and constitutive modelling of ductile high strength steel for a wide range of strain rates," *Int. J. Impact Eng.*, pp. 401-433, 2005.

[44] N. Gebbeken, S. Greulich and A. Pietzsch, "Hugoniot properties for concrete determined by full-scale detonation experiments and flyer-plate-impact tests," *Int. J. Impact Eng.*, vol. 32, pp. 2017-2031, 2006.

[45] S. J. Hiermaier, Structures Under Crash and Impact, Freiburg: Springer, 2008.

[46] S. P. Marsh, LASL Shock Hugoniot Data, Berkeley and Los Angeles: University of California Press Ltd., 1980, p. 658.

[47] F. M. Albakri, "Investigations Of The Effect Of Pressing Conditions On The Physical Mechanical And Ballistic Properties Of Ultra-high Molecular Weight Polyethylene," Master thesis Cranfield University, 2001.

[48] T. A. Bogetti, M. Walter, J. Staniszewski and J. Cline, "Interlaminar shear characterization of ultra-high molecular weight polyethylene (UHMWPE) composite laminates," *Composites Part A: Applied Science and Manufacturing*, vol. 98, pp. 105-115, 2017.